IEEE Access
Multidisciplinary ⋮ Rapid Review ⋮ Open Access Journal

Received 14 June 2024, accepted 7 July 2024, date of publication 10 July 2024, date of current version 29 July 2024.

Digital Object Identifier 10.1109/ACCESS.2024.3425868

RESEARCH ARTICLE

Robust Mass Estimation for Enhanced Braking Distance Calculation in Electric Vehicles With Autonomous Emergency Braking Systems

SANGJIN KO[1], (Member, IEEE), HEE BEOM LEE[1], GYUWON KIM[1], (Member, IEEE), SEUNG-YONG LEE[2], AND GI-WOO KIM[2], (Member, IEEE)
[1]Global Research and Development Center, HL Mando, Pangyo, Seongnam-si 13486, South Korea
[2]Department of Mechanical Engineering, Inha University, Incheon 22212, Republic of Korea

Corresponding author: Gi-Woo Kim (gwkim@inha.ac.kr)

This work was supported by HL Mando Corporation, South Korea.

ABSTRACT This study presents a preliminary investigation into robust vehicle mass estimation to enhance braking distance calculations for autonomous emergency braking systems. While active research has focused on headway distance estimation, primarily using computer vision systems such as cameras or light detection and ranging, there remains considerable room for improvement in reliable autonomous emergency braking systems. In this study, we propose a novel approach to vehicle mass estimation that leverages vehicle longitudinal dynamics, considering that vehicle mass influences braking distance as well as vehicle velocity. We employ an adaptive extended Kalman filter that combines the capabilities of the extended Kalman filter with a fading factor. This algorithm aims to estimate the time-varying vehicle mass using measurements of vehicle longitudinal velocity and driving torque inputs. Subsequently, the estimated vehicle mass serves as the basis for calculating more accurate braking distances. The proposed vehicle mass estimation algorithm is rigorously simulated using MATLAB/SIMULINK, and it undergoes an in-vehicle test.

INDEX TERMS Braking distance, vehicle longitudinal dynamics, vehicle mass, adaptive extended Kalman filter, in-vehicle test.

I. INTRODUCTION

Road traffic accidents, predominantly crashes, are a significant concern for drivers worldwide, with approximately 1.35 million people killed or disabled each year [1]. Generally, human drivers do not consistently pay close attention to traffic conditions due to numerous distraction factors (e.g., looking at the mirror, adjusting the volume of the audio system, or using a cellular phone), or they may be unable to react promptly due to weather conditions, sudden lighting, or physical aging [2]. To address these issues, an autonomous emergency braking (AEB) system was developed to minimize the possibility of rear-end or turn collisions, assisting drivers in avoiding car accidents and reducing unavoidable dangerous situations [3]. These systems use state-of-the-art technology, commonly employing light detection and ranging (LiDAR) devices, cameras, and radar to detect or scan potential obstacles in emergency braking situations [4]. The AEB system measures the distance between the ego vehicle and the lead vehicle moving in front of the ego (host) vehicle and calculates their relative distance (headway). If the system concludes that the measured relative distance exceeds the predetermined distance, the brake system automatically engages to prevent a potential collision. These AEB systems can also communicate with a vehicle's GPS and use its database of traffic signs and other data to apply the brakes quickly. Most sensor-based AEB systems have their advantages and disadvantages. For example, while radars are quite effective at calculating distance and speed even in adverse weather, they are unable to track if deceleration is greater than one. LiDARs, on the other hand, are capable of precise object detection and can compensate for the disadvantages of using radars, but they are usually expensive.

The associate editor coordinating the review of this manuscript and approving it for publication was Ángel F. García-Fernández.

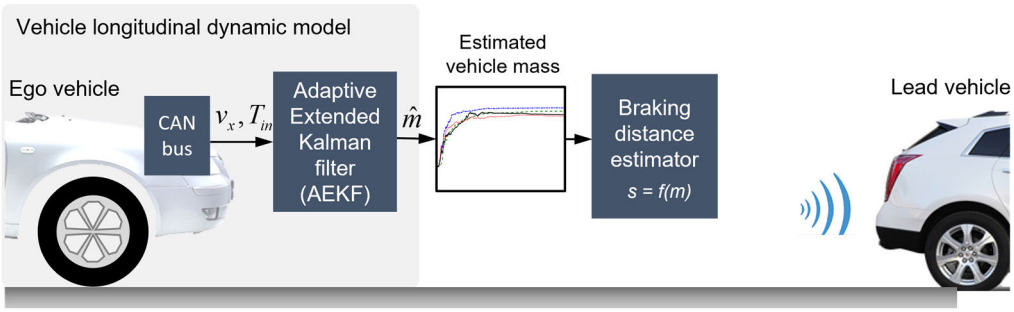

FIGURE 1. Schematic overview of the proposed sensor fusion-based mass estimation for electric vehicles, enhancing braking distance calculation.

In recent years, numerous studies have focused on developing collision warning algorithms alongside advancements in range sensors. These algorithms generally fall into two categories: the safety time algorithm and the safety distance algorithm. The Mazda overriding algorithm introduces a hypothetical worst-case scenario, computing the overriding distance as the minimum range [5]. The safety time logic algorithm compares the collision time between two vehicles with a safety time threshold to determine safety status. Safety time algorithms primarily utilize time-to-collision (TTC) to calculate the remaining time for two vehicles to collide between a leading and following ego (host) vehicle, as depicted in Figure 1 [6]. The Berkeley algorithm suggests a conservative distance to provide a wide range of visual feedback to the driver [7]. The Honda algorithm considers a hypothetical braking scenario [8], while the NHTSA alert algorithm accounts for slightly more complex braking scenarios [9].

However, neither the TTC-based safety time model nor the safe distance model is sufficiently effective in adapting to various braking situations during driving. This is because the traffic and driving environment can be complex, time-varying, and unpredictable. Therefore, the existing collision warning (or avoidance) algorithm is not suitable for rigorous real-world applications. Thus, it is imperative to design a more effective collision warning algorithm that can consider the driving environment. To address the shortcomings of the previously mentioned methods, researchers have attempted to propose new stopping distance-based algorithms. Calculating the safe stopping distance is one of the most effective ways to assess the possibility of a rear-end accident. These techniques for assessing rear-end collision risk are based on the assumption that the leading vehicle's tire friction coefficient must be higher than that of the following host vehicles [6]. Because more accurate braking distance calculation improves collision-warning solutions when stopping at a given vehicle velocity, many researchers have attempted to develop more rigorous collision-warning algorithms based on non-parametric techniques. For example, artificial neural network (ANN)-based technology is one of the most promising alternatives in rear-end collision warning systems [10]. The advantage of the ANN-based approach is its ability to solve complex unobservable problems. Despite active research concerning collision warning algorithms, primarily focusing on effective stopping distance calculation, considerable room for improvement remains.

Real-time monitoring of vehicle states has recently garnered increasing attention due to its critical role in controlling future vehicles, including both autonomous and conventional ones. In particular, vehicle mass is one of the essential parameters in many automotive control systems, as its accuracy directly impacts control performance and robustness. Real-time information on vehicle mass is also vital for fleet management systems. Automotive control systems that demand rigorous real-time vehicle mass information include active safety systems such as the aforementioned collision warning systems [11], active suspension control [12], and electronic stability programs [13] etc. However, determining the actual vehicle mass poses a challenge due to its time-varying nature, depending on factors such as payload, such as the number of passengers, and the amount of fuel. small-size passenger cars, in particular, exhibit a significant ratio between payload and vehicle mass. Moreover, directly measuring vehicle mass using typical mechanical sensors is challenging for control purposes. Conventional vehicle mass estimation methods, such as weighbridges, axle weigh pads, or weigh-in-motion systems, are impractical for non-stationary driving vehicles. Therefore, there is considerable interest in estimating vehicle mass in real time.

Most current techniques for estimating vehicle mass rely on longitudinal and lateral vehicle dynamic models [14], [15], [16], [17], [18], [19], [20], [21], [22], [23]. Sensor fusion data for estimating vehicle mass can be provided by the vehicle controller area network (CAN) bus, resulting in cost-effective implementation. Rigorous vehicle mass estimation requires real-time information on vehicle variables such as longitudinal acceleration, road grade, and driving torque. Additionally, numerous studies have attempted to simultaneously estimate road grade using state-of-the-art technology such as a two-antenna global navigation satellite system (GNSS) and road map [24]. However, longitudinal vehicle dynamics suffer from various system information and unknown

disturbance inputs known as road loads, such as gradient due to gravitational force, aerodynamic drag, and rolling resistance. Some research on vehicle mass estimation has been proposed based on a vertical dynamic system [25]. Jordan et al. [26] proposed a vehicle mass estimator using a multi-model filter based on the vertical dynamic system to reduce the effort of a calibrated referenced dual Kalman filter for estimating road irregularities and vehicle mass. Using inertial measurement units (IMUs) can be an alternative approach [27]. The accelerometer inside the IMU can then be used to provide longitudinal vehicle acceleration instead of relying on the time derivative of vehicle speed from the CAN bus, resulting in inaccurate acceleration estimates.

In this study, vehicle mass estimation for enhanced braking distance calculation in electric vehicles with AEB systems is explored based on the fact that braking distance is affected by vehicle mass [28]. Thus, we develop an indirect sensor fusion-based vehicle mass estimation approach using an adaptive extended Kalman filter (AEKF), which combines the capabilities of the extended Kalman filter with a fading factor. This approach aims to enhance braking distance calculation for AEB systems by considering the dependence of braking distance on both vehicle mass, as depicted in Figure 1. To our knowledge, there are no reports detailing the possibility of achieving an improved collision warning algorithm by considering vehicle mass. Therefore, the objective of this study is to propose a new mass estimation method to enhance the braking distance calculation required for the collision warning algorithm of AEB systems. The remainder of this study is organized as follows: Section II outlines the braking distance calculation, focusing on the effect of vehicle mass on the braking distance of AEB systems. Section III presents the detailed AEKF algorithm, and the proposed algorithm is experimentally validated in in-vehicle tests in Section IV.

II. BRAKING DISTANCE ANALYSIS

A. NEW BRAKING DISTANCE MODEL

To analyze the sensitivity of vehicle mass on braking distance, we first formulate a new safe distance model for vehicles. This model assumes that both vehicles start from the same initial velocity and experience the same deceleration. Typically, the conventional safe distance is modeled by the following simple formula based on physics, specifically the mechanical energy conservation law [2]:

$$s = v_c t_d + \left(\frac{v_c^2}{2\mu g} - \frac{v_l^2}{2\mu g}\right) = v_c t_d + \left(\frac{v_c^2}{2a_c} - \frac{v_l^2}{2a_l}\right) \quad (1)$$

where v_c denotes the controlled (host, ego) vehicle velocity; v_l denotes the lead vehicle velocity; t_d is the delay time, which consists of human delay plus judgment time (i.e., free running), μ represents the tire friction coefficient, a_c and a_l denote the deceleration limit parameters, which are usually assumed to be the same but can vary (e.g. 4.6 for dry road, 3.3 for wet road).

In this study, a new safe distance model was formulated by considering only the braking distance (i.e., the second part of Eq. (1)). As depicted in Figure 2, the net force applied to a vehicle driving in the longitudinal direction can be governed by

$$\gamma_m m\dot{v} = F_x - F_b - 0.5\rho C_d A_f v^2 - f_r mg\cos\theta - mg\sin\theta \quad (2)$$

where v is the vehicle longitudinal velocity, F_x denotes the tire tractive force, F_b denotes the braking force, γ_m denotes the mass factor for the equivalent mass considering the moment of inertia, ρ denotes the density of air, C_d denotes the aerodynamic drag coefficient, A_f denotes the vehicle frontal area, f_r represents the rolling resistance coefficient, m represents the vehicle mass to be estimated in this study, and θ represents the inclined angle. Assuming that the vehicle is driving on a flat road ($\theta = 0$) during braking ($F_x = 0$), Eq. (2) can be simplified as

$$\gamma_m mv\frac{dv}{ds} = -F_b - 0.5\rho C_d A_f v^2 - f_r mg \quad (3)$$

The braking distance s can then be calculated by integrating the infinitesimal distance element ds derived from Eq. (3) as

$$s = \int_{v_1}^{v_2} ds = \frac{\gamma_m m}{\rho C_d A_f}\ln\left(1 + \frac{\rho C_d A_f v_1^2}{2(\eta_b\mu mg + f_r mg)}\right) \quad (4)$$

where $F_b = \eta_b\mu mg$, v_1 denotes the initial velocity, v_2 the final velocity ($v_2 = 0$), and η_b the braking efficiency (assumed) [29]. All vehicle parameters for the simulation are listed in Table 1. Braking distances were simulated using different vehicle masses ($v_1 = 30\ m/s$). The braking distance increases as the vehicle mass increases, whereas it decreases as the tire friction coefficient increases, as shown in Figure 3.

TABLE 1. Parameters for braking distance calculation.

Symbol	Parameters	Value
γ_m	Mass factor	1.15
f_r	Rolling resistance coefficient	0.004
C_d	Aerodynamic drag coefficient	0.4
η_b	Braking efficiency	0.5
A_f	Vehicle's frontal area	3 m^2
ρ	Density of air	1.293 kg/m^3

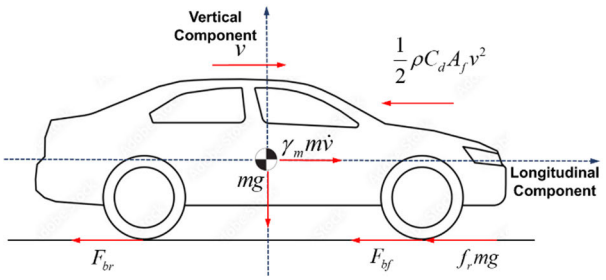

FIGURE 2. Schematic illustration of longitudinal vehicle dynamics.

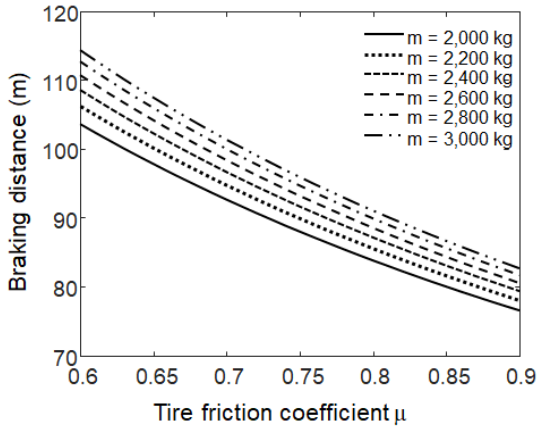

FIGURE 3. Braking distance calculation with respect to different vehicle masses ($v_1 = 30\ m/s$, $v_2 = 0$).

B. NONLINEAR SIMULATION OF BRAKING DISTANCE

The braking distance of a passenger car equipped with anti-skid braking system (ABS) was simulated to conservatively evaluate the effect of vehicle mass on the braking distance. The wheel dynamics is then required to consider the slipping behavior of the wheel.

$$\dot{\omega}_w = \left[T_e - T_b - r_w F_x - T_w\left(\omega_w\right)\right]/J_w \tag{5}$$

where ω_w denotes the wheel velocity, T_e denotes the engine input torque, T_b denotes the braking torque, r_w denotes the wheel radius, and $T_w\left(\omega_w\right)$ denotes a wheel-friction torque, J_w is the inertia moment of the wheel. The tire tractive force is defined as:

$$F_x = \mu(\lambda) F_z \tag{6}$$

where F_z is the normal force at each tire, μ is the tire friction coefficient and a function of slip ratio $\lambda = (x_2 - x_1)/x_1$ for braking (so-called simple magic formula or Pacejka model [2]). The wheel-friction torque is assumed to be the combination of dry-friction and viscous-friction models

$$T_w\left(\omega_w\right) = f_w F_z + b_w \omega_w \tag{7}$$

The actuator dynamics is also considered by modeling as the 1st order system as follows;

$$\dot{T}_b = -\left(1/\tau\right) T_b + k F_a \tag{8}$$

where τ is the time constant, k is the actuator gain, F_a is the actuation force. Then, the governing equation of motion can be formulated by defining $x_1 = \omega_v, x_2 = \omega_w$, $x_3 = T_b$.

$$\begin{aligned}
\dot{x}_1 &= \left[-(0.5\rho C_d A_f)(r_w x_1)^2 + N_w F_z \mu(\lambda)\right]/(\gamma_m m r_w) \\
\dot{x}_2 &= \left[-f_w F_z - b_w x_2 - F_z r_w \mu(\lambda) + T\right]/J_w \\
\dot{x}_3 &= -\left(1/\tau\right) x_3 + k F_a
\end{aligned} \tag{9}$$

where $T = T_e - T_b$, N_w is the total number of wheel. For the ABS ($\lambda > 0$), a simple two-stage on-off ABS controller was designed

$$e = \lambda_d - \lambda \tag{10}$$

$$F_a = \begin{Bmatrix} F_{a\_\max}, e(t) > 0 \\ F_{a\_\min}, e(t) < 0 \end{Bmatrix} \tag{11}$$

where e is the error defined by the difference between the desired slip ratio $\lambda_d (= 0.2)$ and actual slip ratio λ.

The nonlinear simulation was performed by numerically integrating Eq. (9) (Runge-Kutta 4th-order method). Wheel velocity fluctuated with the frequency of 5 Hz due to the on-off control and actuator dynamics, as shown in Figure 4 (a), which shows a good agreement with in-vehicle test results (5∼ 10 Hz). The slip ratio was regulated around the desired slip ratio of 0.2, as shown in Figure 4 (c). The braking distance can be calculated by integrating the area in Figure 4 (b). Obviously, the braking distance increased as increased the vehicle mass, and shows a good agreement with simulated values using CarSim, as shown in Figure 4 (d). The braking distance ranges from 50 m to 60 m when the vehicle mass varies from 2500 kg to 2950 kg. As described in previous Section, the braking distance difference of 10 m is significant and will affect the accuracy of the AEB system and needs to be compensated.

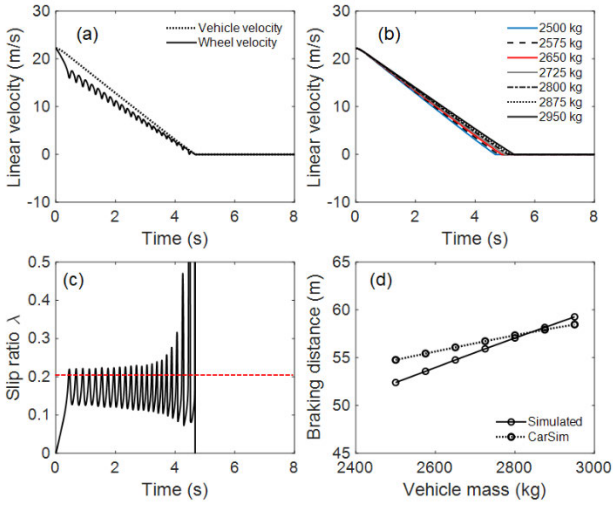

FIGURE 4. Simulation result of braking distance; (a) time history of two velocities, (b) time history of vehicle velocity with varying vehicle masses, (c) slip ratio history, and (d) simulated braking distance vs vehicle mass.

III. DESIGN OF VEHICLE MASS ESTIMATOR

A. LONGITUDINAL VEHICLE MODEL

Assuming that the braking force is inactive and the algorithm operates solely during driving, the governing equation can be further simplified as follows:

$$\gamma_m m \dot{v} = F_x - 0.5\rho C_d A_f v^2 - f_r m g \tag{12}$$

Compared to conventional vehicles with internal combustion engines combined with multi-stepped automatic

transmissions, the tractive force of electric vehicles can be determined by the kinematics of gear and wheels

$$F_x = \frac{T_m G \eta}{R} \tag{13}$$

where T_m denotes the motor output torque, G denotes the reduction gear ratio (10.65), η denotes the mechanical efficiency, and R denotes the effective radius of the wheel. Introducing the additional assumption that the vehicle mass is in a quasi-static state ($\dot{m} \approx 0$), the governing equation can be expressed as follows:

$$\dot{x} = f(x,u) = \begin{bmatrix} \dot{x}_1 \\ \dot{x}_2 \end{bmatrix} = \begin{bmatrix} \frac{F_x}{m} - \frac{\rho C_d A_f}{2m} v^2 - g f_r \\ 0 \end{bmatrix} \tag{14}$$

$$\boldsymbol{x} = \begin{bmatrix} x_1 & x_2 \end{bmatrix} = \begin{bmatrix} v & m \end{bmatrix}^T \quad , \quad y = v = x_1 \tag{15}$$

The reformulated system model is nonlinear, and the output measurement is the longitudinal velocity of the vehicle.

B. AEKF

In this study, we utilize an extended Kalman filter (EKF) to estimate the time-varying parameter of vehicle mass within nonlinear longitudinal dynamics by linearizing a nonlinear model at equilibrium points. Additionally, we propose an adaptive EKF (AEKF) with a fading factor to enhance estimation performance [30], [31]. The equations for AEKF are identical to those of the conventional AEKF in equations, except for the modification involving the fading factor ($\lambda \geq 1$) in the error covariance equation. As a result, the latest measured data is given greater weight in the state estimation, thereby preventing divergence. As the proposed AEKF algorithm operates in the discrete-time domain, we discretize the continuous equation using the Euler method. This is expressed as

$$\dot{x} = \frac{x(k) - x(k-1)}{\Delta t} \rightarrow x(k) = \dot{x}(k)\Delta t + x(k-1) \tag{16}$$

where Δt is the time step and k and $k-1$ represent the time instants at $t = k\Delta t$ and $t = (k-1)\,\Delta t$, respectively. Substituting Eq. (14) into Eq. (16), Eq. (15) is defined as follows:

$$\begin{cases} x_k = f_{k-1}(x_{k-1}, u_{k-1}) \\ y_k = h(x_k) \end{cases} \tag{17}$$

The general linear discrete-time system model required to design the KF is given by

$$\begin{aligned} x_{k+1} &= Ax_k + Bu_k + w_k \\ y_k &= Hx_k + v_k \end{aligned} \tag{18}$$

where w_k is a multivariate Gaussian distribution system noise variable with covariance matrix, and v_k is a multivariate Gaussian distribution measurement noise variable with covariance matrix. In this study, no input was applied to the measurement model, and the application of the EKF was based on the nonlinear model. The general discrete-time equation is as follows:

$$\begin{cases} x_k = f_{k-1}(x_{k-1}, u_{k-1}) + w_{k-1} \\ y_k = h(x_k) + v_k \end{cases} \tag{19}$$

The extended Kalman filter assumes the differentiability of the state-change function instead of the linearity of the model.

$$A_{k-1} = \left.\frac{\partial f_{k-1}}{\partial x}\right|_{\hat{x}_{k-1}}, B_{k-1} = \left.\frac{\partial f_{k-1}}{\partial u}\right|_{\hat{x}_{k-1}}, H_k = \left.\frac{\partial h_k}{\partial x}\right|_{\hat{x}_{k|k-1}} \tag{20}$$

The nonlinear system model was linearized using a Jacobian matrix calculated based on the previous estimate. Matrices A and H of the rotating-shaft system model were linearized using Eq. (20) and are expressed as follows:

$$\begin{aligned} A_{k-1} &= \begin{bmatrix} 1 - \frac{\rho C_d A_f x_1}{x_2}\Delta t & -\left(\frac{F_x}{x_2^2} + \frac{\rho C_d A_f x_1^2}{2x_2^2}\right)\Delta t \\ 0 & 1 \end{bmatrix} \\ H_k &= \begin{bmatrix} 1 & 0 \end{bmatrix} \end{aligned} \tag{21}$$

C. FADING FACTOR UPDATE

To optimally select the fading factor to minimize g_k, we introduced the adaptive rule called p-adaptation [32].

$$\lambda_k^{l+1} = \lambda_k^l + \varphi \frac{\partial g_{\lambda,k}^l}{\partial \lambda_k^l} \; \forall l = 0, 1, 2, \cdots, \tag{22}$$

where the subscript k represents the time series, the superscript l represents the number of iterations in a time instant, and φ is the step length (i.e., learning rate) for the gradient descent method. The constant fading factor is optimally updated to identify and track a time-varying parameter. At the p-th iteration, if the fading factor converges, the iteration is terminated, and the optimal fading factor is determined by

$$\lambda_k = \max\left\{1, \lambda_k^p\right\} \tag{23}$$

However, this iterative numerical method can fail to obtain an explicit formula for the optimal calculation of λ_k, and its real-time implementation is challenging. Consequently, a one-step AEKF algorithm was employed to reduce the computational burden in this study [27]. Assuming that Q_k, R_k, and P_0 are positive definite, and that the measurement matrix H_k is full rank, the fading factor can be reformulated as

$$\lambda_k = \max\left\{1, trace\left[N_k\right] / trace[M_k]\right\} \tag{24}$$

where

$$M_k = H_k A_{k,k-1} P_{k-1}^+ A_{k,k+1}^T H_k^T, \text{ and} \tag{25}$$

$$N_k = C_{0,k} - H_k Q_{k-1} H_k^T - R_k. \tag{26}$$

The fading factor can then be adaptively determined when the difference between the N_k(present state) and M_k(past state) becomes larger (i. e., sudden state variation) using the

three consecutive recursive equations with initial conditions $G_{1,0} = 0$ and $G_{2,0} = 0$.

$$C_{0,k} = G_{1,k} / G_{2,k} \tag{27}$$

$$G_{1,k} = G_{1,k-1} / \lambda_{k-1} + z_k z_k^T \tag{28}$$

$$G_{2,k} = G_{2,k-1} / \lambda_{k-1} + 1 \tag{29}$$

The mathematical proof and details of this algorithm are presented in [27]. Under the established conditions, the estimation error of vehicle mass is bounded, provided that the initial error and noise terms remain within acceptable limits. Consequently, the stability of the mass estimation algorithm is proved [33]. The overall estimation process using the AEKF algorithm with a fading factor update is illustrated in Figure 5.

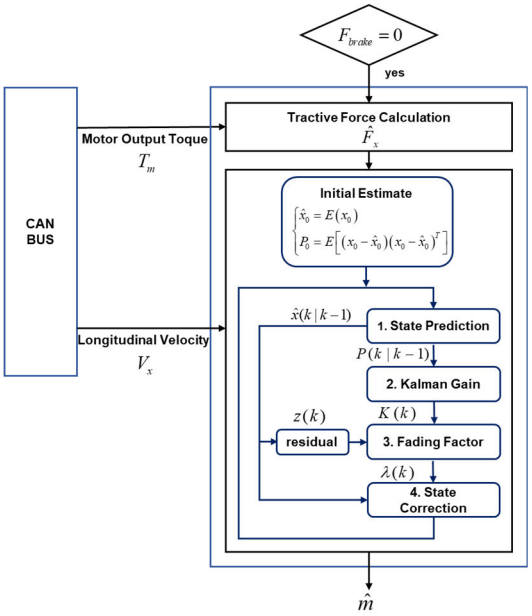

FIGURE 5. The overall estimation process using the AEKF algorithm.

D. SIMULATION RESULTS

Based on the proposed algorithm, a vehicle-driving scenario was simulated using MATLAB®. The system model parameters are listed in Table 1. In this study, the step response to a sudden upward step input was used to evaluate the response time of the proposed estimator. The initial state value and error covariance for the estimation are as follows:

$$x_0 = [\,0 \;\; 2000\,], \;\; P_0 = diag([\,10000 \;\; 10000\,]) \tag{30}$$

The system noise covariance matrix Q and measurement noise covariance R were tuned in various cases as follows, and the optimal estimates were derived:

$$Q = diag\left[\,10^{-8} \;\; 10^{-8}\,\right], \;\; R = 0.00001 \tag{31}$$

To evaluate the basic estimation performance of the AEKF, the root-mean-squared error (RMSE) at the kth time instant was calculated for a more rigorous analysis.

$$RMSE(k) = \sqrt{\frac{1}{k}\sum_{i=1}^{k}(p(i) - \hat{p}(i))^2} \tag{32}$$

where $p(i)$ and $\hat{p}(i)$ represent the true and estimated values, respectively. The steady-state mean of the RMSE (MRMSE) was then calculated to exclude the effects of transient behavior. Typical estimation results are illustrated in Figure 6. The AEKF (initial mass of 2470 kg) accurately tracked the vehicle mass variation from 2540 kg (two passengers) to 2680 kg (three passengers). As shown in Figure 6 (a), the conventional EKF cannot track the time-varying vehicle mass.

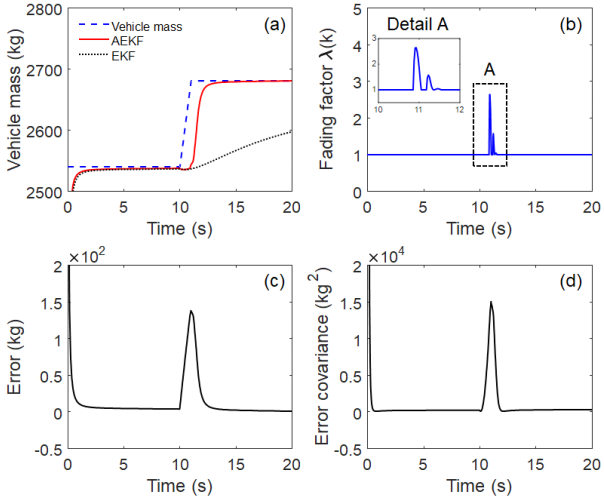

FIGURE 6. Simulation result of vehicle mass estimation; (a) responses of time-varying vehicle mass to slew rate limited input (mass increase), (b) time evolution of the fading factor (inset, detail around mass change), (c) estimation error (AEKF) and (d) convergence history of error covariance.

Although the sensor signals were contaminated by random Gaussian noise, the proposed AEKF successfully tracked the time-varying vehicle mass. The estimation performance of the proposed AEKF model was evaluated under parametric uncertainties, such as the system noise covariance matrix Q. The nominal value of the system noise covariance matrix Q ($10^{-8} \cdot I_{2\times2}$) is perturbed by $10^{-9} \cdot I_{2\times2}$ and $10^{-7} \cdot I_{2\times2}$, respectively. The estimation results varied from the nominal values under various parametric uncertainties, as depicted in Figure 7. When reducing Q ($10^{-9} \cdot I_{2\times2}$) below its nominal value, the response time is almost no difference compared to the result of the nominal value, but the overshoot notably increases. Accordingly, the magnitude of the fading factor peaked compared to the nominal at the mass change point. Conversely, increasing Q ($10^{-7} \cdot I_{2\times2}$) beyond the nominal value reduces overshoot, while the response time significantly increases to the extent that it is difficult to estimate. As illustrated by the estimation results in Figure 7, the importance of appropriately setting the system matrix can be observed in evaluating the performance of the algorithm.

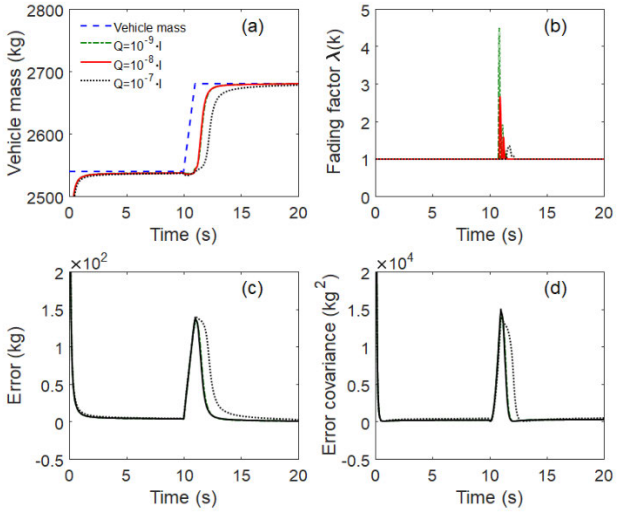

FIGURE 7. Simulation result of vehicle mass estimation with different system noise covariance matrix Q; (a) responses of time-varying vehicle mass to slew rate limited input (mass increase), (b) time evolution of the fading factor (inset, detail around mass change), (c) estimation error (with different Q), and (d) convergence history of error covariance.

IV. EXPERIMENTAL VALIDATION

A. IN-VEHICLE TEST

The in-vehicle test system was designed to validate the proposed algorithm. It comprises a ground electric vehicle (model: SUV, curb weight: 2230 kg), data acquisition devices, a computer with vehicle network processors (model: NXP S32G, and a display for monitoring, as shown in Figure 8b. Two measurement signals for KF-UI (drive motor output torque and longitudinal velocity) were collected via the controller area network flexible data rate (CAN FD) bus protocol. To facilitate this communication protocol, a compact CAN FD interface device (model: Kvaser) was used, connecting the host PC to the high/low channels of the CAN FD bus. Non-uniformly sampled signals were resampled with uniform sampling time (0.005 s). All algorithms in Python were executed on a Linux platform in real time. During the in-vehicle test, the algorithm was activated only when regenerative braking is off and the vehicle is accelerating. Variable vehicle mass was made possible by sequentially changing the number of passengers at stopping and represented by four scenarios: CASE A (four passengers + payload), CASE B (four passengers), CASE C (three passengers), and CASE D (two passengers), respectively.

FIGURE 8. Schematic representation of the in-vehicle test: (a) interior space, (b) equipment, and (c) test bed vehicle overview.

B. SYSTEM IDENTIFICATION

In this study, the recursive least squares estimator (RLSE) was adopted to identify unknown parameters of the vehicle longitudinal model. As the performance of a vehicle mass estimator largely depends on the accuracy of the model parameters, an offline system identification process is required. To design the RLSE, a longitudinal vehicle model (Eq. (12) is reformulated in matrix form as

$$\boldsymbol{y}_k = \boldsymbol{h}_k^T \boldsymbol{\theta}_k + \boldsymbol{v}_k \tag{33}$$

where

$$\boldsymbol{y}_k = F_x \boldsymbol{h}_k^T = \left[\, \dot{v} \;\; v^2 \;\; 1 \,\right], \text{ and } \boldsymbol{\theta}_k = \left[\, \hat{m} \;\; \hat{C}_d \;\; \hat{F}_r \,\right]^T \tag{34}$$

The system is represented by a linear model in the form of Eq. (33), where $\boldsymbol{y}_k$ denotes the output vector and $\boldsymbol{h}_k^T$ represents the measurement matrix, which are known values that can be obtained by processing sensor signals. Also, $\boldsymbol{\theta}_k$ denotes the unknown parameter vector to be estimated. $\boldsymbol{v}_k$ is measurement noise. F_r represents the rolling resistance force, which expressed as $f_r mg$ in Eq. (12). The numerical values for $\boldsymbol{y}_k$ and $\boldsymbol{h}_k^T$ can be measured directly using the CAN data acquired from the driving vehicle. The RLSE was designed as follows [34]:

1) Initial estimates

$$\hat{\theta}_0 = E\left[\theta\right] \tag{35}$$

$$P_0 = E\left[\left(\theta - \hat{\theta}_0\right)\left(\theta - \hat{\theta}_0\right)^T\right] \tag{36}$$

2) Kalman-gain calculation

$$K_{k+1} = P_k \boldsymbol{h}_{k+1} \left(\boldsymbol{h}_{k+1}^T P_k \boldsymbol{h}_{k+1} + \boldsymbol{w}_{k+1}^{-1}\right)^{-1} \tag{37}$$

3) Parameter update

$$\hat{\boldsymbol{\theta}}_{k+1} = \hat{\boldsymbol{\theta}}_k + K_{k+1}\left(\boldsymbol{y}_{k+1} - \boldsymbol{h}_{k+1}^T \hat{\boldsymbol{\theta}}_k\right) \tag{38}$$

4) Covariance update

$$P_{k+1} = \left(I - K_{k+1} \boldsymbol{h}_{k+1}^T\right) P_k \tag{39}$$

In the first step, the estimated parameter and its covariance are initialized to arbitrary values as they are usually unknown. The estimated parameter vector θ_k is then calculated by Eqs. (37), (38), and (39), updating at each time step in a recursive manner, where $\boldsymbol{w}_k$ signifies system noise. The four measured in-vehicle data identified system parameters are illustrated in Figure 9 and Figure 10, respectively. The three parameters were successfully estimated, converging over time to a certain finite steady state, as summarized in Table 2. The profile of the tractive force in Figure 10 (d) was calculated by substituting identified parameters into Eq. (33), and nearly coincides with the vehicle longitudinal acceleration in Figure 9 (b).

TABLE 2. Identified system parameters.

Symbol	Parameters	Value
m	Vehicle mass (nominal)	2707 kg
F_r	Rolling resistance force	566.3 N
C_d	Aerodynamic drag coefficient	0.69

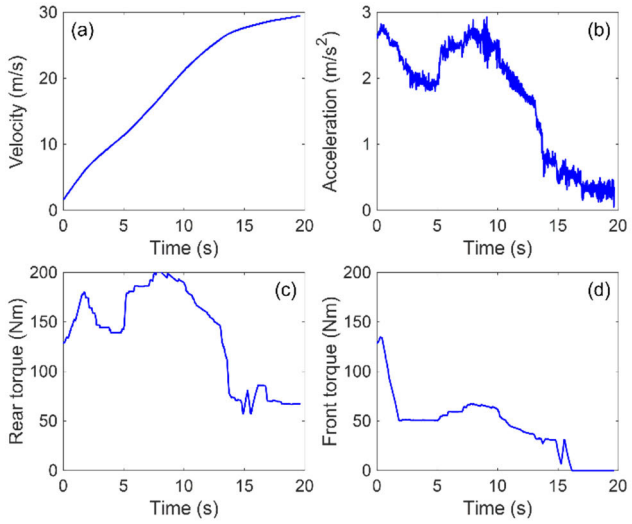

FIGURE 9. Measured in-vehicle data (acceleration 0→ 30 m/s (100 km/h)) (a) vehicle longitudinal velocity (b) vehicle longitudinal acceleration (c) rear motor torque, and (d) front motor torque.

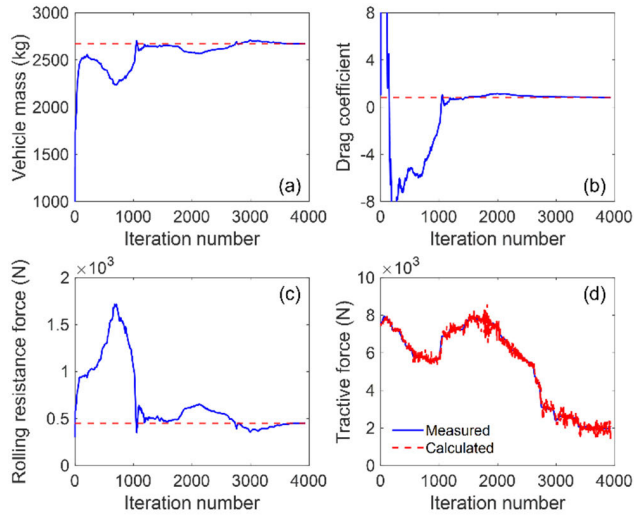

FIGURE 10. System identification results (0→ 30 m/s (100 km/h)) (a) vehicle mass, (b) aerodynamic drag coefficient, and (c) rolling resistance force, (d) comparison of calculated and measured tractive force.

C. RESULTS AND DISCUSSION

Upon comparing the vehicle mass estimation, including transient responses, it becomes evident that the proposed estimation algorithm effectively captures the steady-state vehicle mass response caused by four scenarios, as depicted Figure 11 (a). From the transient responses to sudden mass variation (similar to a step input), the algorithm can quickly track the variable vehicle mass (i.e., within 2 s). The proposed vehicle mass detection method tracks four cases of mass variation (CASE A, B, C, and D) with relatively large initial estimation error (initial mass estimate: 1200 kg). For a more rigorous analysis, MRMSE for steady state response between 3 to 6 seconds is calculated using Eq. (32) and presented in Table 3. Through the calculated MRMSE values, it can be confirmed that the final estimated mass values (CASE A: 2880 kg, CASE B: 2811 kg, CASE C: 2722 kg, CASE D: 2652 kg) for all case scenarios exhibit a high level of accuracy, with errors within 2 % compared to the actual values. In particular, compared to the conventional EKF where the covariance matrix P is not updated using the fading factor, a notable difference in convergence speed from initial estimation value to steady state can be observed (i.e., 2.66 s). The fading factor history of the vehicle mass estimation of the AEKF algorithm is shown in Figure 11 (b). The fading factor is adaptively updated to better suit the initial tracking of the vehicle mass estimation.

TABLE 3. Comparison of MRMSE.

	AEKF	AEKF (with noise)	EKF
CASE A	17.753	25.568	77.499
CASE B	32.635	49.909	108.571
CASE C	3.552	24.620	106.794
CASE D	13.566	27.230	46.908

The robustness of the proposed estimation model under noise uncertainty is analyzed by introducing perturbation of sensor noises and system parameters. Since sensor information is inherently contaminated by electrical noises, the effect of electrical noise on the estimation performance was examined. White Gaussian random noise was added to all sensor data. For example, the probability density function of motor torque and vehicle velocity including white Gaussian random noise is shown in Figure 12. Because the random noise (error) distribution can be fitted to a normal Gaussian distribution with the variance ($\sigma^2 = 0.15$, Motor torque, $\sigma^2 = 0.1$, Vehicle velocity), as shown in Figure 12 (b) and d, it was confirmed to be white Gaussian random noise. The experimental results show good robustness against Gaussian random noise, as shown in Figure 13. The robustness of the proposed algorithm in terms of the fading factor is further demonstrated by comparing its history as depicted in Figure 11 (b) and Figure 13 (b). It can be observed that the fading factor is updated more frequently with larger values, compensating for uncertainty in the model resulting in fast adaptation to noise. Consequently, the estimation error shows no significant change, as listed in Table 3. The convergence speed of the proposed algorithm can be further improved by replacing the initial mass estimation value of 1200 kg with a more reasonable vehicle mass value (e.g., 2500 kg). Based on the sensitivity analysis of vehicle mass and braking

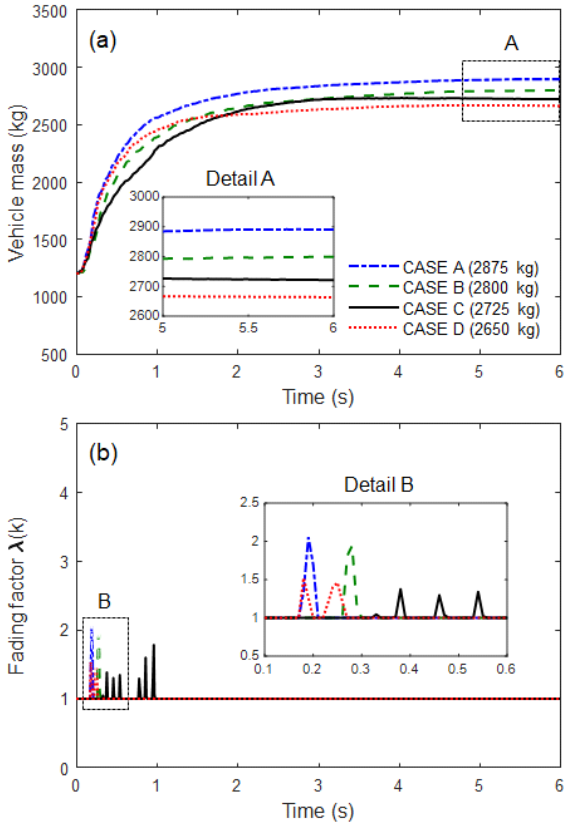

FIGURE 11. Comparison of vehicle mass estimation responses corresponding to four CASES (inset: zoomed of A, B).

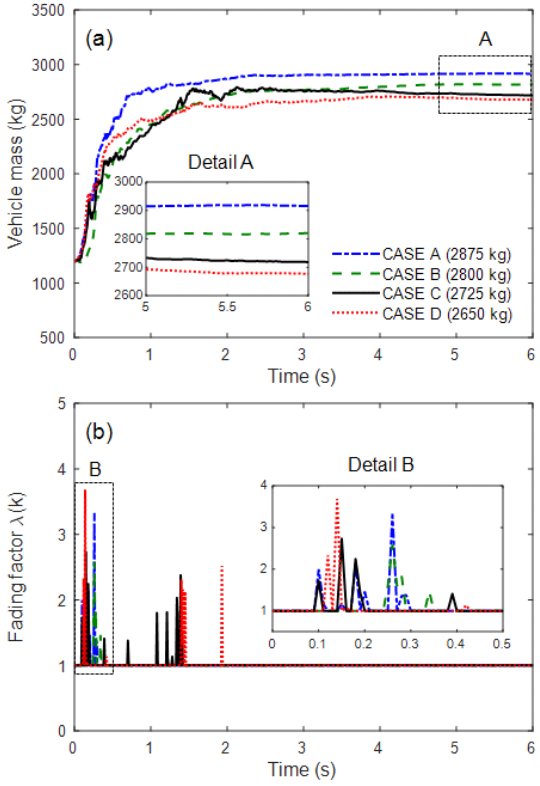

FIGURE 13. Comparison of vehicle mass estimation responses corresponding to four CASES (inset: zoomed of A, B).

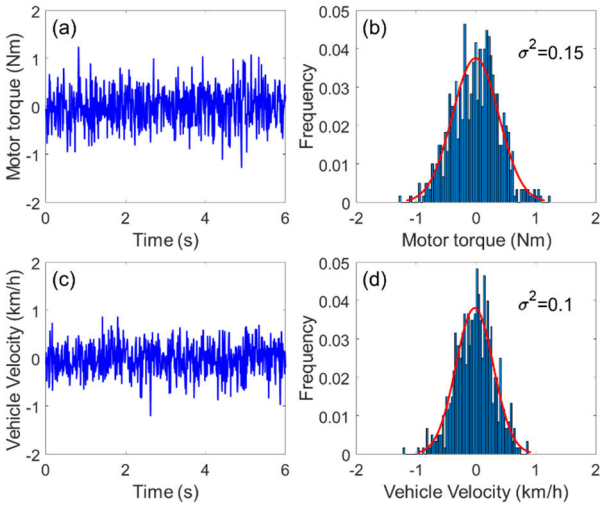

FIGURE 12. Gaussian random noises for robustness analysis: (a) motor torque noise (more contaminated), (b) its histogram, (c) vehicle velocity noise (less contaminated), (d) its histogram.

distance in Section II, it is noted that there is an increased sensitivity between braking distance and mass, especially on low-friction roads where the maximum braking distance can vary by up to 147 meters. Therefore, it is important to accurately estimate mass variations which can vary up to 300 kg due to additional passengers and luggage within the vehicle. Consequently, accurate mass estimation from the proposed AEKF algorithm is anticipated to have a significant impact when integrated into future AEB algorithms.

However, there is still a need to enhance the robustness of the proposed algorithm against uncertainties. In particular, the tractive force is highly sensitive to various road conditions. The kinematics between torque and tractive force in Eq. (13) can only be available under the assumption of no-slip conditions. This assumption may affect the estimation performance under dynamic driving conditions such as slipping. Such issues can be addressed either by utilizing an additional wheel dynamic model in the algorithm or by only activating algorithm when no slipping. Initial conditions also impact the convergence rate of AEKF. Although initial conditions can be reasonably approximated (e.g., by using the vehicle's curb weight), the convergence rate can significantly vary in the general EKF. In contrast, the proposed AEKF can robustly estimate the vehicle mass by utilizing a fading factor, thereby addressing model uncertainties.

V. CONCLUSION

In this study, we have successfully developed a new vehicle mass estimation method based on adaptive extended Kalman filtering of vehicle longitudinal dynamics. The main contributions are summarized as follows:

- Firstly, to the best of our knowledge, we report for the first time that it is possible to enhance braking distance calculations for autonomous emergency braking systems by estimating vehicle mass using measurements of vehicle longitudinal velocity and driving torque inputs of electric vehicles. Subsequently, the estimated vehicle mass serves as the basis for calculating more accurate braking distances. In addition, our proposed vehicle mass estimation method has an advantage over conventional methods owing to its simplicity and robustness.
- Secondly, the proposed method exhibits high potential for advancing the accuracy of AEB systems by considering the real variable vehicle mass.
- Lastly, another advantage of AEKF for electric vehicles is that only two pieces of sensor information (drive motor output torque and longitudinal velocity) are required via the CAN FD bus for our approach, whereas the estimation of output torque is extremely complicated in conventional vehicles (i.e., those based on internal combustion engines).

However, there is still a need to enhance the robustness of the proposed algorithm against noise and parametric uncertainties. For future research, we will address these ongoing issues. Our focus will be on advancing the algorithm for AEB systems to calculate more accurate braking distances, thereby enhancing the reliability and robustness of the AEB system. Additionally, we plan to apply our new approach to various vehicular electronics applications in autonomous vehicles by substituting constant vehicle mass with variable vehicle mass.

ACKNOWLEDGMENT

The authors are grateful to engineers Jong-Ik Won (HL Mando) and Yeon-Su Sim (Inha University) for their assistance with the data collection during the in-vehicle tests.

REFERENCES

[1] S. K. Ahmed, M. G. Mohammed, S. O. Abdulqadir, R. G. A. El-Kader, N. A. El-Shall, D. Chandran, M. E. U. Rehman, and K. Dhama, "Road traffic accidental injuries and deaths: A neglected global health issue," *Health Sci. Rep.*, vol. 6, no. 5, p. e1240, May 2023.

[2] A. G. Ulsoy, H. Peng, and M. Çakmakci, *Automotive Control Systems*. Cambridge, U.K.: Cambridge Univ. Press, 2012.

[3] J. B. Cicchino, "Effectiveness of forward collision warning and autonomous emergency braking systems in reducing front-to-rear crash rates," *Accident Anal. Prevention*, vol. 99, pp. 142–152, Feb. 2017.

[4] M. Ariyanto, G. D. Haryadi, M. Munadi, R. Ismail, and Z. Hendra, "Development of low-cost autonomous emergency braking system (AEBS) for an electric car," in *Proc. 5th Int. Conf. Electr. Veh. Technol. (ICEVT)*, Oct. 2018, pp. 167–171.

[5] O. Ararat, E. Kural, and B. A. Guvenc, "Development of a collision warning system for adaptive cruise control vehicles using a comparison analysis of recent algorithms," in *Proc. IEEE Intell. Vehicles Symp.*, Sep. 2006, pp. 194–199.

[6] I.-C. Han, B.-C. Luan, and F.-C. Hsieh, "Development of autonomous emergency braking control system based on road friction," in *Proc. IEEE Int. Conf. Autom. Sci. Eng. (CASE)*, Aug. 2014, pp. 933–937.

[7] P. Seiler, B. Song, and J. K. Hedrick, "Development of a collision avoidance system," *SAE Trans.*, vol. 107, pp. 1334–1340, Jan. 1998.

[8] Y. Zhang, "Engineering design synthesis of sensor and control systems for intelligent vehicles," Ph.D. dissertation, California Inst. Technol., Pasadena, CA, USA, 2006.

[9] S. Brunson, E. Kyle, N. Phamdo, and G. Preziotti, "Alert algorithm development program: NHTSA rear-end collision alert algorithm," Nat. Highway Traffic Saf. Admin., Washington, DC, USA, Tech. Rep., 2002.

[10] D. Lee and H. Yeo, "A study on the rear-end collision warning system by considering different perception-reaction time using multi-layer perceptron neural network," in *Proc. IEEE Intell. Vehicles Symp. (IV)*, Jun. 2015, pp. 24–30.

[11] X.-Y. Lu and J. Wang, "Multiple-vehicle longitudinal collision avoidance and impact mitigation by active brake control," in *Proc. IEEE Intell. Vehicles Symp.*, Jun. 2012, pp. 680–685.

[12] V. K. Maurya and N. S. Bhangal, "Optimal control of vehicle active suspension system," *J. Autom. Control Eng.*, vol. 6, no. 1, pp. 22–26, 2017.

[13] D. Yin, N. Sun, and J.-S. Hu, "A wheel slip control approach integrated with electronic stability control for decentralized drive electric vehicles," *IEEE Trans. Ind. Informat.*, vol. 15, no. 4, pp. 2244–2252, Apr. 2019.

[14] N. Lin, C. Zong, and S. Shi, "The method of mass estimation considering system error in vehicle longitudinal dynamics," *Energies*, vol. 12, no. 1, p. 52, Dec. 2018.

[15] S. Kim, K. Shin, C. Yoo, and K. Huh, "Development of algorithms for commercial vehicle mass and road grade estimation," *Int. J. Automot. Technol.*, vol. 18, no. 6, pp. 1077–1083, Dec. 2017.

[16] M. Zhao, F. Yang, D. Sun, W. Han, F. Xie, and T. Chen, "A joint dynamic estimation algorithm of vehicle mass and road slope considering braking and turning," in *Proc. Chin. Control Decis. Conf. (CCDC)*, Jun. 2018, pp. 5868–5873.

[17] G. Reina, M. Paiano, and J.-L. Blanco-Claraco, "Vehicle parameter estimation using a model-based estimator," *Mech. Syst. Signal Process.*, vol. 87, pp. 227–241, Mar. 2017.

[18] E. J. Holm, "Vehicle mass and road grade estimation using Kalman filter," *Inst. Syst. Dep. Electr. Eng*, vol. 16, pp. 1–38, Jan. 2011.

[19] N. Kidambi, R. L. Harne, Y. Fujii, G. M. Pietron, and K. W. Wang, "Methods in vehicle mass and road grade estimation," *SAE Int. J. Passenger Cars-Mech. Syst.*, vol. 7, no. 3, pp. 981–991, Apr. 2014.

[20] A. Jo, Y. Jeong, H. Lim, and K. Yi, "Vehicle mass and road grade estimation for longitudinal acceleration controller of an automated bus," *J. Auto-Vehicle Saf. Assoc.*, vol. 12, no. 2, pp. 14–20, 2020.

[21] M. N. Mahyuddin, J. Na, G. Herrmann, X. Ren, and P. Barber, "Adaptive observer-based parameter estimation with application to road gradient and vehicle mass estimation," *IEEE Trans. Ind. Electron.*, vol. 61, no. 6, pp. 2851–2863, Jun. 2014.

[22] Y. Zhang, Y. Zhang, Z. Ai, Y. Feng, J. Zhang, and Y. L. Murphey, "Estimation of electric mining haul Trucks' mass and road slope using dual level reinforcement estimator," *IEEE Trans. Veh. Technol.*, vol. 68, no. 11, pp. 10627–10638, Nov. 2019.

[23] N. Kidambi, G. M. Pietron, M. Boesch, Y. Fujii, and K.-W. Wang, "Accuracy and robustness of parallel vehicle mass and road grade estimation," *SAE Int. J. Vehicle Dyn., Stability, NVH*, vol. 1, no. 2, pp. 317–325, Mar. 2017.

[24] H. S. Bae, J. Ryu, and J. C. Gerdes, "Road grade and vehicle parameter estimation for longitudinal control using GPS," in *Proc. IEEE Conf. Intell. Transp. Syst.*, Jun. 2001, pp. 25–29.

[25] H. Yang, B.-G. Kim, J.-S. Oh, and G.-W. Kim, "Simultaneous estimation of vehicle mass and unknown road roughness based on adaptive extended Kalman filtering of suspension systems," *Electronics*, vol. 11, no. 16, p. 2544, Aug. 2022.

[26] J. Jordan, N. Hirsenkorn, F. Klanner, and M. Kleinsteuber, "Vehicle mass estimation based on vehicle vertical dynamics using a multi-model filter," in *Proc. 17th Int. IEEE Conf. Intell. Transp. Syst. (ITSC)*, Oct. 2014, pp. 2041–2046.

[27] K. M. Jensen, I. F. Santos, L. K. H. Clemmensen, S. Theodorsen, and H. J. P. Corstens, "Mass estimation of ground vehicles based on longitudinal dynamics using loosely coupled integrated navigation system and CAN-bus data with model parameter estimation," *Mech. Syst. Signal Process.*, vol. 171, May 2022, Art. no. 108925.

[28] W. Luty, "Simulation-based analysis of the impact of vehicle mass on stopping distance," *Eksploatacja i Niezawodnos˙c-Maintenance Rel.*, vol. 20, no. 2, pp. 182–189, Jun. 2018.

[29] D. K. Murthy and A. Masrur, "Exploiting space buffers for emergency braking in highly efficient platoons," in *Proc. IEEE 23rd Int. Conf. Embedded Real-Time Comput. Syst. Appl. (RTCSA)*, Aug. 2017, pp. 1–10.

[30] T.-S. Lou, Z.-H. Wang, M.-L. Xiao, and H.-M. Fu, "Multiple adaptive fading Schmidt–Kalman filter for unknown bias," *Math. Problems Eng.*, vol. 2014, no. 1, 2014, Art. no. 623930.

[31] L. Ozbek and F. A. Aliev, "Comments on adaptive fading Kalman filter with an application," *Automatica*, vol. 34, no. 12, pp. 1663–1664, 1998.
[32] C.-H. Loh, C.-Y. Lin, and C.-C. Huang, "Time domain identification of frames under earthquake loadings," *J. Eng. Mech.*, vol. 126, no. 7, pp. 693–703, Jul. 2000.
[33] K. H. Kim, J. G. Lee, C. G. Park, and G. I. Jee, "The stability analysis of the adaptive fading extended Kalman filter," in *Proc. IEEE Int. Conf. Control Appl.*, Oct. 2007, pp. 982–987.
[34] J. M. Mendel, *Lessons in Estimation Theory for Signal Processing, Communications, and Control*. London, U.K.: Pearson, 1995.

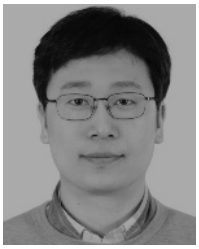

SANGJIN KO (Member, IEEE) received the B.S. degree from Ajou University, in 2006, the M.S. degree from Korea Advanced Institute of Science and Technology (KAIST), in 2008, and the Ph.D. degree in mechanical engineering from Texas A&M University, in 2021. He is a Senior Engineer with HL Mando Corporation. Previously, he was an Assistant Research Engineer with Hyundai Mobis. His research interest includes artificial intelligence for advanced control applications.

HEE BEOM LEE received the B.S. degree in mechanical engineering from Inha University, Incheon, South Korea, in 2021, and the M.S. degree in mechanical engineering from Inha University, in 2023. He is currently a Research Engineer with HL Mando Corporation.

GYUWON KIM (Member, IEEE) received the B.S. degree in mechanical engineering from Pohang University of Science and Technology (POSTECH), in 2020, and the M.S. degree in mechanical engineering from Inha University, in 2022. He is a Research Engineer with HL Mando Corporation, where he is in alternative military service for the Republic of Korea Armed Forces as a Technical Research Personnel. His current research focuses on the foundational theory and interdisciplinary practice of artificial intelligence-of-things (AIoT) to advance synergistic applications across various engineering domains.

SEUNG-YONG LEE received the B.S. degree in mechanical engineering from Inha University, Incheon, South Korea, in 2024, where he is currently pursuing the M.S. degree with the Control Systems and Mechatronics Laboratory. His research interests include Kalman filters, parameter estimation, vehicle control, and their industrial applications.

GI-WOO KIM (Member, IEEE) received the Ph.D. degree from the Mechanical Engineering Department, The Pennsylvania State University, USA, in 2009. He held positions with the Powertrain Research and Development Center, Hyundai Motor Company, from 1996 to 2004; and the Mechanical Engineering Department, University of Michigan, from 2009 to 2011. Following this, he was an Assistant Professor with Kyungpook National University, from 2011 to 2015. From September 2015 to February 2021, he was an Associate Professor with Inha University, where he has been a Professor, since March 2021. His research interests include data-driven mechanical engineering, machine learning, measurement and control, vehicular electronics, and related fields.